Structure-Activity Relationship Studies and Biological Characterization of Human NAD+-dependent 15-Hydroxyprostaglandin Dehydrogenase Inhibitors

Damien Y. Duveau[a], **Adam Yasgar**[a], **Yuhong Wang**[a], **Xin Hu**[a], **Jennifer Kouznetsova**[a], **Kyle R. Brimacombe**[a], **Ajit Jadhav**[a], **Anton Simeonov**[a], **Craig J. Thomas**[a], and **David J. Maloney**[a,*]

David J. Maloney: maloneyd@mail.nih.gov

[a]National Center for Advancing Translational Sciences, National Institutes of Health, 9800 Medical Center Drive, Rockville, MD, 20850

Abstract

The structure-activity relationship (SAR) study of two chemotypes identified as inhibitors of the human NAD+-dependent 15-hydroxyprostaglandin dehydrogenase (HPGD, 15-PGDH) was conducted. Top compounds from both series displayed potent inhibition (IC_{50} <50 nM), demonstrate excellent selectivity towards HPGD and potently induce PGE_2 production in A549 lung cancer and LNCaP prostate cancer cells.

Keywords

HPGD; 15-PGDH; prostaglandin; PGE_2; inhibitor

Introduction

Prostaglandins are members of the eicosanoid family of signaling molecules, along with lipoxins and leukotrienes. They are synthesized from arachidonic acid (AA), which following its release from membrane phospholipids, undergoes a series of transformations mediated by enzymes such as cyclooxygenases (COX) and prostaglandin synthases. Prostaglandins are also inactivated through chemical modification. One key metabolizing enzyme is 15-hydroxyprostaglandin dehydrogenase (HPGD, also referred to as 15-PGDH), which catalyzes the oxidation of the prostaglandin hydroxyl group at C-15 to the corresponding ketone.[1]

A number of prostaglandins of particular biological interest have been identified as substrates of HPGD. Prostaglandin E_2 (PGE_2), a product of COX-2-mediated AA metabolism via prostaglandin H_2 (PGH_2) is converted by HPGD to its biologically inactive metabolite, 15-keto-PGE_2. Over-production of PGE_2 has been reported to promote tumor-associated neovascularization, cell proliferation, and tumor growth.[2] It has also been suggested that decreased levels of PGE_2 resulting from amplified HPGD activity through

pharmacological means or enhanced expression may mitigate these phenotypes and result in a chemoprevention strategy.[3] Conversely, HPGD was found to be highly expressed in androgen receptor-overexpressing advanced tumors, metastatic prostate cancers,[4] and metastatic breast cancer, where it has been found to contribute to epithelial-mesenchymal transition (EMT). [5] 15-deoxy-$\Delta^{12,14}$-prostaglandin J_2 (15d-PGJ$_2$) is a product of albumin-mediated transformation of prostaglandin D_2 (PGD$_2$), itself derived from PGH$_2$.[6] 15d-PGJ$_2$ was shown to inhibit IKKβ, a positive regulator of NF-κB,[7,8] and to covalently bind Keap1, a negative regulator of Nrf2.[9] As such, the metabolism of PGD$_2$ by HPGD provides a possible link between HPGD activity and levels of 15d-PGJ$_2$. Moreover, Blair et al. recently demonstrated that HPGD catalyzed the transformation of 11-hydroxy-eicosatetranoic acid (11-HETE), a product of COX-2/HPGD-mediated AA transformation, into 11-oxo-eicosatetranoic acid (11-oxo-ETE),[10] and that 11-oxo-ETE inhibits NF-κB signaling through inhibition of IKKβ.[11] Therefore, down regulation of HPGD may lead to a decrease in the NF-κB signaling pathway and to an increase in Nrf2 signaling.

As a consequence of prostaglandins' roles in a number of processes such as inflammation, differentiation, and cellular signaling, their cellular levels are tightly regulated. The central role of HPGD to inactivate prostaglandins such as PGE$_2$ or PGD$_2$ makes it an important target for pharmacological intervention. Prior to our efforts, few inhibitors of HPGD have been identified, and all are based off ciglitazone, a PPARγ inhibitor possessing a thiazolidinedione scaffold. The parent compound was found to have an IC$_{50}$ against HPGD of 2.7 μM[12] whereas an optimized analogue, CT-8, displayed an IC$_{50}$ of 51 nM.[13] More recently, the same group continued their SAR studies around ciglitazone and related analogues, with demonstrated activity *in vivo* for their top compounds,[14] but the selectivity of CT-8 toward other dehydrogenases was not reported. In addition, the thiazolidinedione chemotype is likely to have undesired off-target effects given the well documented PPARγ activity for this class of molecules.

In an effort to identify selective inhibitors of HPGD, we conducted a quantitative high throughput screen (qHTS) of ~160,000 compounds as part of the Molecular Libraries Small Molecule Repository (MLSMR). These studies led to the identification of three structurally distinct small molecule chemical probes as potent and selective inhibitors of HPGD (denoted as **ML147**, **ML148**, and **ML149**, Fig. 1).[15] The first scaffold, **ML147**, is characterized by an azabenzimidazole core appended with a thiobenzyl group at C-1. The second compound, **ML148** possesses a benzimidazole core substituted with a cyclohexylamide moiety and 3-methyl-phenyl group. Finally, **ML149** contains a triazoloazepine core with 2,5-dimethylpyrrole group linked to the triazole ring. Given the potential liabilities (e.g. glutathione reactivity) of the thiol ether linkage on **ML147** we decided to focus our initial SAR efforts on the optimization of **ML148** and **ML149**. In addition to our SAR efforts, we also sought to define key *in vitro* ADME properties, cellular efficacy (PGE$_2$ levels) and selectivity against several related dehydrogenases (*vide infra*).

Optimization of ML149

In order to support compound scale-up for more detailed biological testing and to facilitate SAR explorations, we designed concise synthetic routes to **ML148**, **ML149** and related analogues. Our initial efforts were focused on **ML149** as shown in Scheme 1.

The carboxylic acid functionality of commercially available pyrrole **1** (Scheme 1) was activated using carbonyldiimidazole (CDI) in THF and the resulting acylimidazole was then treated with hydrazine monohydrate to afford hydrazide **2**. This reaction was performed on a two-gram scale, and the product was isolated from the imidazole (reaction by-product) by recrystallization in ethyl acetate. Treatment of hydrazide **2** with 1-aza-2-methoxy-1-

cycloheptene in chlorobenzene in a microwave (MW) reactor led to formation of triazole **3** in 71% yield. Finally, Ullman-type coupling between **3** and iodobenzene afforded **ML149**. The use of 4,7-dimethoxy-1,10-phenanthroline (L) as a copper ligand allowed for the efficient activation of the air-stable metal catalyst;[16] furthermore, using polyethylene glycol (PEG) as a co-solvent improved the solubilization of the inorganic base and of the copper salt, accounting for the improved performance of the reaction.[17] Using this synthetic sequence, eighteen analogues (**4a-r**) with differentially substituted *N*-pyrrole aromatic rings were synthesized (Table 1).

Overall, the substitution at the *meta or para* position of the *N*-pyrrole phenyl ring with small substituents provided analogues with activities comparable to that of **ML149**, however, some subtle SAR trends emerged. Modification of the *para* position with a halogen group led to analogues with slightly improved potencies [**4a** (3,4-dichloro-phenyl), **4c** (4-Cl-phenyl and **4d** (4-Br-phenyl)], with bis-substituted analogue **4a** being the most potent (IC$_{50}$ = 22 nM). However, introduction of other electron-withdrawing groups at the *para* position such as F (**4e**), CF$_3$ (**4g**), CN (**4j**) and NO$_2$ (**4l**), resulted in a slight loss of potency. We did find that the phenyl ring could not be replaced by a heterocycle, such as a pyridine ring (compounds **4o-q**) without a more significant drop in potency. Of note, a number of phenyl analogues bearing *ortho* substituents could not be successfully synthesized, likely because the steric hindrance of the two pyrrole methyl groups prevent the Ullman-type coupling reaction from taking place.

The synthetic sequence outlined in Scheme 1 is ideal for late-stage diversification of the pendant aryl ring but is less optimal for investigations of the triazoloazepine core. For facile preparation of these analogues we utilized common intermediate **2**, followed by cyclization with various 1-aza-2-methoxy derivatives **5a-e** to ultimately provide five analogues (**6a-d**) with rings of various sizes fused to the triazole moiety (Scheme 2).

Upon biological testing of the compounds, no direct correlation was found between the sizes of the ring fused to the triazole moiety and HPGD activity (Table 1). However, the five-membered ring analogue **6a** resulted in a significant loss of potency (IC$_{50}$ = 3.04 μM) suggesting the importance of having at least a 6-membered fused ring. Whereas, the 6-(**6b**), 8-(**6c**) and 9-membered (**6d**) ring analogues were less active than **ML149**. Having completed our initial SAR investigations of the core and pendant phenyl ring, we then wanted to probe the influence of the substituents on the pyrrole ring (Table 1). The synthesis of these compounds was achieved in a manner similar to the analogues described previously, except the starting carboxylic acid was varied (Scheme 3).

The unsubstituted pyrrole **7a** displayed a six-fold drop in activity (IC$_{50}$ = 607 nM) as compared to **ML149**, highlighting the importance of substitution on the pyrrole. The indole derivative (**7c**) was less active (IC$_{50}$ = 681 nM), and the addition of other heteroatoms were not tolerated [e.g. pyrrazole derivative **7b** (IC$_{50}$ = 3.83 μM)].

Optimization of ML148

Following the optimization of **ML149**, which led to the identification of compounds **4a** (IC$_{50}$ = 22 nM) and **4b** (IC$_{50}$ = 34 nM), we turned our attention to benzimidazole-based chemotype **ML148**. The synthesis route was optimized in order to provide rapid access to a variety of analogues as shown in Scheme 4.

Benzoic acid **8** was treated with *m*-toluidine in *N*-methylpyrolidinone (NMP) to afford intermediate **9**. The nitro group was reduced using hydrazine and Raney nickel (Ra-Ni) in methanol to afford the crude 3-amino-4-(m-tolylamino)benzoic acid which was then

converted to benzimidazole **10** via treatment with triethylorthoformate and catalytic *p*-toluenesulfonic acid (TsOH) in THF. This synthetic sequence was carried out on a gram-scale, and no flash chromatography or HPLC purification was required to isolate any of the synthetic intermediates. Finally, treatment of carboxylic acid **10** with a range of amines (R_1R_2NH), using HATU and diisopropylethylamine (DIPEA) in DMF provided a library of 14 analogues of **ML148** (compounds **11a-n**) possessing differing amide moieties. Unfortunately, none of these compounds resulted in improved potency (Table 2); however, it did provide key information regarding the steric requirements around the cyclohexylamide functionality. A smaller ring (**11i**) or an exocyclic amine (**11k**) led to compounds with decreased activity (20-50 fold respectively). Substituents at the 3-position on the piperidine ring were well tolerated (**11a** and **11c-e**), including the relatively bulky isopropyl group (**11c**). While adding a 4-Br group (**11f**) only led to a modest decrease in potency, the 4-CF_3 group led to a drastic loss of potency (80-fold) compared to the corresponding 3-CF_3 (**11e**). Moreover, the presence of heteroatoms (N or O) at the 4-position was also not well tolerated, with activity in the micromolar range (**11m**: N-Me-Piperazine) or inactivity (**11n**: morpholine). Finally, acyclic amides (**11h** and **11l**) were much less active than cyclic ones, and secondary amides (**11k** and **11l**) were less active than tertiary amides (**11h**). In order to explore SAR around the *N*-linked phenyl ring of **ML148**, we wanted to devise a route in which the varying phenyl groups could be introduced in the last step. As such, benzoic acid **8** was treated with oxalyl chloride and a small amount of DMF in dichloromethane, and the resulting acyl chloride was treated with piperidine-hydrochloride in dichloromethane to afford amide **12** (Scheme 4). The remainder of the synthesis proceeded as planned, starting with substitution of the aromatic fluorine with various amines (R_3NH_2) in the presence of DIPEA in DMF to provide anilines **13a-n**. The aromatic nitro group was reduced, and the resulting anilines were treated with triethylorthoformate as described above to afford analogues **14a-n**.

Analogues **14a-n** displayed activities similar to that of **ML148** (Table 2) with relatively flat SAR being observed. Introduction of a small substituents in *para-* and in *meta*-position afforded compounds with similar activities, whereas electron-withdrawing groups (**14e** and **14k**) and bulkier substituents (**14f,g,l**) in *para-* and in *meta*-position resulted in a loss of potency.

Inporation of non-aromatic groups (**14m,n**) had minimal effect on the potency. These data suggest that this region could be exploited for future modulation of ADME properties since it appears very tolerant to change. However, it remains unclear whether introduction of a hydrophilic group will be tolerated since all analogues prepared thus far are generally lipophilic in this region.

ADME profile

To assess the potential for these compounds to be used *in vivo,* we obtained *in vitro* ADME properties of a few selected analogues of the **ML149** and **ML148** chemotypes (Table 3).

In general, **ML149** and related analogues showed good kinetic solubility (>28 μM in phosphate buffered saline (PBS) at pH 7.4). Results from the PAMPA assay, which measures passive (artificial) membrane permeability, showed that halogen substituents seem to improve permeability (e.g. compounds **4a** and **4b**). On the other hand, substitution with a nitrile moiety led to a ten-fold drop in permeability (**4i**). Unfortunately, **ML149** and its analogues degraded quickly in the presence of rat liver microsomes, as evidenced by their short half-life (<10 min). **ML148** and its analogues also displayed good kinetic solubility (>47 μM), except for compound **11d** (5.6 μM). PAMPA permeability of **ML148** and related

analogues was similar to the **ML149** series. As with **ML149**, the rat liver microsomal stability remained undesirable, except for compound **14j** ($T_{1/2}$ = 23 min).

Selectivity toward HPGD

In order to evaluate the selectivity of the prepared compounds toward HPGD, analogues of **ML148** and of **ML149** were tested for their inhibitory activities versus a panel of five other dehydrogenases (Supplemental Table 1).[18] Encouragingly, none of the compounds tested showed any activity against GAPDH, LDHA, LDHB and HSD17β4. Some inhibition was observed against ALDH1 A1, though all compounds displayed considerable selectivity toward HPGD (greater than 28-fold selectivity). Analogues **4b** (142-fold selectivity), **14c** (160-fold selectivity), and **14e** (142-fold selectivity) were the most selective HPGD inhibitors.

PGE$_2$ production

A selection of top actives around the **ML148** and **ML149** chemotypes were tested for their ability to increase PGE$_2$ levels. Lung cancer A549 cells and androgen-sensitive human prostate adenocarcinoma LNCaP cells were titrated with the selected HPGD inhibitors; the half-maximal activation concentration (AC_{50}) and percentage induction (% Induction) of PGE$_2$ production are reported in Table 4.

All the compounds tested increased PGE$_2$ production levels when compared to a DMSO control, in both A549 cells and LNCaP cells. The percent induction was consistently higher in A549 cells (from 106% for **ML149** to 174% for **14j**) than in LNCaP cells (from 44% for **4f** to 105% for **4a**). The majority of the compounds tested displayed sub-micromolar activity in both cell lines, and a good correlation in AC_{50} was observed between the two cell lines: low AC_{50} values measured in A549 cells correlated with low AC_{50} values in LNCaP cells, with the exception of **ML149** [AC_{50} = 0.743 μM (A549) and AC_{50} = 2.80 μM (LNCaP)] and of **11d** [AC_{50} = 0.743 μM (A549) and AC_{50} = 4.43 μM (LNCaP)]. Unfortunately, no tractable SAR emerged from the PGE$_2$ production assay, a likely consequence of the often diverging enzymatic potency and cell permeability properties of the inhibitors. Indeed, compound **4i** displayed particularly low cell permeability in the PAMPA assay (229×10^{-6} cm/s), probably accounting for the low activity measured in the A549 (AC_{50} = 2.64 μM) and LNCaP (AC_{50} = 1.77 μM) cell lines. It is also possible that enzyme occupancy of different agents and the kinetics of the sequential enzymatic events adds a level of complexity that may account for these differences. Overall, the data obtained in the PGE$_2$ production assay showed that treatment with our inhibitors leads to increased PGE$_2$ production in A549 lung cancer and in LNCaP prostate cancer cells, consistent with inhibition of HPGD in the cell.

Conclusion

The structure-activity relationship (SAR) study of two small molecule inhibitors of the human HPGD, **ML148** and **ML149**, was carried out. These studies revealed that while the fused seven-membered ring and the presence of a 2,5-dimethylpyrrole were required for activity of **ML149**, a certain tolerance in the substitution pattern of the phenyl ring was observed. As a result compound **4h** was found to have improved potency toward HPGD, improved cell permeability and induced PGE$_2$ production both in A549 and in LNCaP cells, when compared to **ML149**. For the benzimidazole chemotype (**ML148**), the cyclohexylamide group was found to be optimal for enzymatic activity, although small substituents at the 3-position of the cyclohexyl amine group were tolerated. Moreover, substitution at the *meta*-position of the phenyl ring was also well-tolerated, leading to analogues **14c** and **14j**. Both compounds displayed similar ADME properties, although **14j**

was more stable in the RLM assay, and both analogues had comparable effects on PGE_2 levels in A549 and in LNCaP cells. Unfortunately, none of the HPGD inhibitors tested led to any observable down regulation of NF-κB, as measured in our assay (Supplemental Figure 1), perhaps due to compensatory mechanisms counteracting the effect of modulation of HPGD activity on NF-κB regulation. In conclusion, we have identified potent and selective inhibitors of HPGD (e.g. **4h** and **14j**) and hope these compounds help better define the role of HPGD in a variety of diseases. As such, we make these compounds freely available to the research community upon request.

Supplementary Material

Refer to Web version on PubMed Central for supplementary material.

Acknowledgments

References

1. Tai HH, Cho H, Tong M, Ding Y. Curr Pharm Design. 2006; 12:955.

2. Wang D, DuBois RN. Gut. 2006; 55:115. [PubMed: 16118353]

3. Na HK, Park JM, Lee HG, Myung SJ, Surh YJ. Biochem Pharmacol. 2011; 82:1352. [PubMed: 21856294]

4. Vainio P, Gupta S, Ketola K, Mirtti T, Mpindi JP, Kohonen P, Fey V, Perälä M, Smit F, Verlaegh G, Schalken J, Alanen KA, Kallioniemi O, Iljin K. Am J Pathol. 2011; 178:525. [PubMed: 21281786]

5. Lehtinen L, Vainio P, Wikman H, Reemts J, Hilvo M, Issa R, Pollari S, Brandt B, Oresic M, Pantel K, Kallioniemi O, Iljin K. J Pathol. 2012; 226:674. [PubMed: 22072156]

6. Surh YJ, Na HK, Park JM, Lee HN, Kim W, Yoon IS, Kim DD. Biochem Pharmacol. 2011; 82:1335. [PubMed: 21843512]

7. Straus DS, Pascual G, Li M, Welch JS, Ricote M, Hsiang CH, Sengchanthalangsy LL, Ghosh G, Glass CK. Proc Natl Acad Sci USA. 2000; 97:4844. [PubMed: 10781090]

8. Trivedi SG, Newson J, Rajakariar R, Jacques TS, Hannon R, Kanaoka Y, Eguchi N, Colville-Nash P, Gilroy DW. Proc Natl Acad Sci USA. 2006; 103:5179. [PubMed: 16547141]

9. Oh JY, Giles N, Landar A, Darley-Usmar V. Biochem J. 2008; 411:297. [PubMed: 18237271]

10. Liu X, Zhang S, Arora JS, Snyder NW, Shah SJ, Blair IA. Chem Res Toxicol. 2011; 24:2227. [PubMed: 21916491]

11. Snyder, NW.; Revello, SD.; Liu, X.; Zhang, S.; Arora, JS.; Blair, IA. Presented at the AACR 103rd Annual Meeting; Chicago, IL. March 31 – Apr 4, 2012;

12. Cho H, Tai HH. Prostaglandins Leukot Essent Fatty Acids. 2002; 67:461. [PubMed: 12468268]

13. Cho H, Tai HH. Arch Biochem Biophys. 2002; 405:247. [PubMed: 12220539]

14. Wu Y, Karna S, Choi CH, Tong M, Tai HH, Na DH, Jang CH, Cho H. J Med Chem. 2011; 54:5260. [PubMed: 21650226]

15. Niesen FH, Shultz L, Jadhav A, Bhatia C, Guo K, Maloney DJ, Pilka ES, Wang M, Oppermann U, Heightman TD, Simeonov A. Plos One. 2010; 5:e13719. [PubMed: 21072165]

16. Altman RA, Buchwald SL. Org Lett. 2006; 8:2779. [PubMed: 16774255]

17. Altman RA, Koval ED, Buchwald SL. J Org Chem. 2007; 72:6190. [PubMed: 17625886]

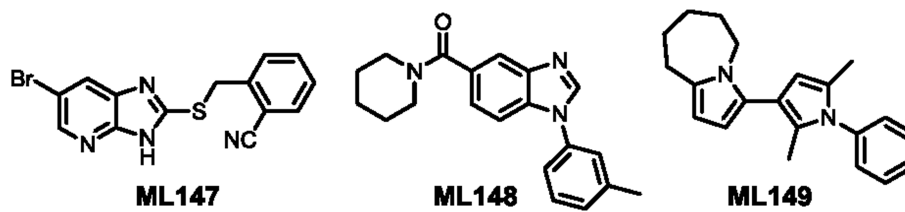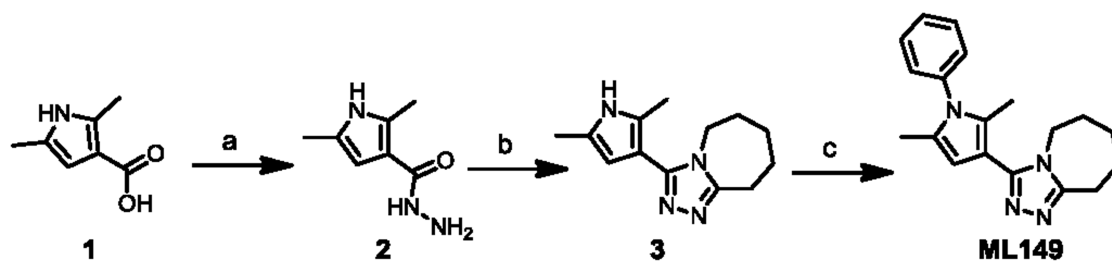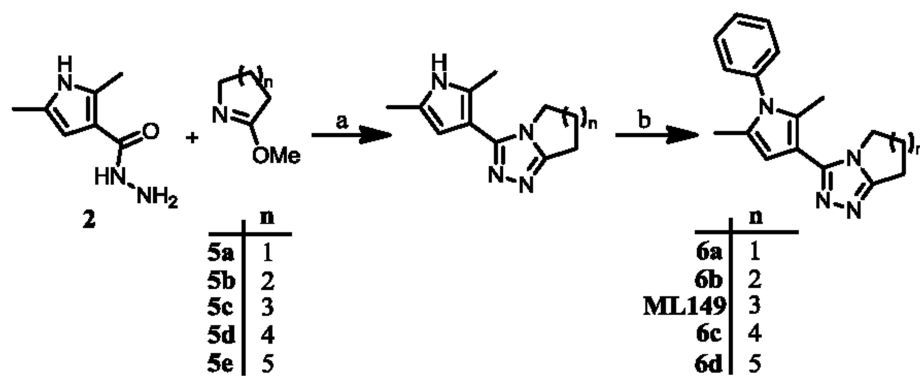18. The activity data of **ML148** and of **ML149** versus ALDH1A1, HADH2 and HSD17β4 were reported in reference 15.
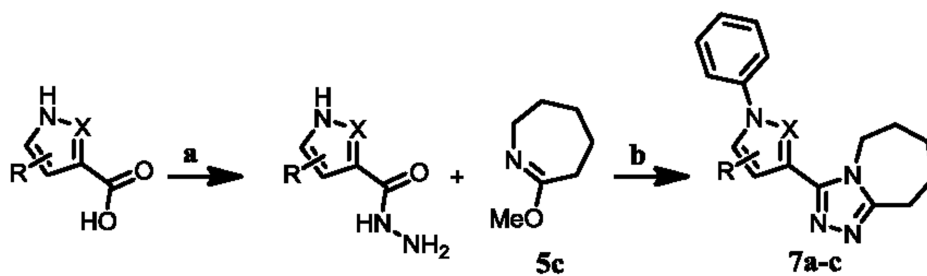
Figure 1.
Structures of chemotypes **ML147**, **ML148**, and **ML149**.

Scheme 1.
Reagents and conditions: (a) CDI, THF, then hydrazine-hydrate, 23 °C, 3.5 h, 65%; (b) 1-aza-2-methoxy-1-cycloheptene, PhCl, MW, 180 °C, 45 min, 71%; (c) PhI, Cs_2CO_3, Cu_2O, 4,7-dimethoxy-1,10-phenanthroline, NMP-PEG, 100 °C, 16 h, 44%.

Scheme 2.
Reagents and conditions: (a) PhCl, MW, 180 °C, 45 min; (b) PhI, Cs_2CO_3, Cu_2O, L, NMP-PEG, 80-100 °C, 16 h.
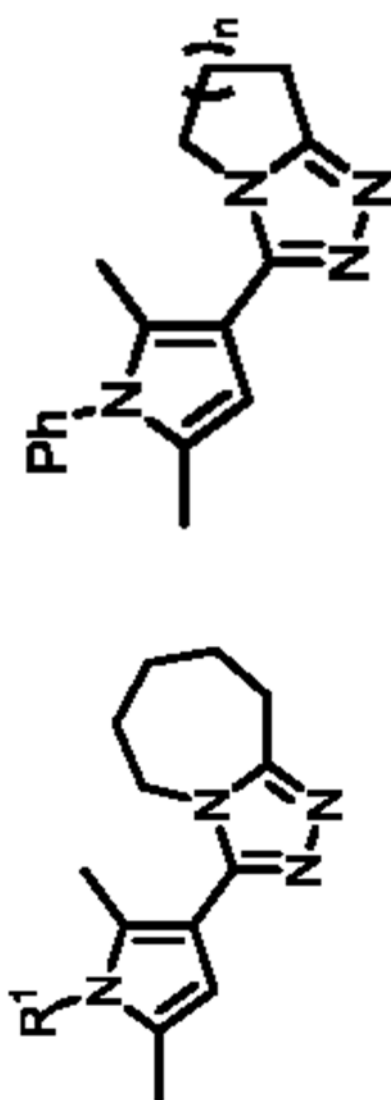
Scheme 3.
Reagents and conditions: (a) CDI, THF, then hydrazine-hydrate, 23 °C; (b) (1) 1-aza-2-methoxy-1-cycloheptene, PhCl, MW, 180 °C; (2) PhI, Cs_2CO_3, Cu_2O, L, NMP-PEG, 100 °C.
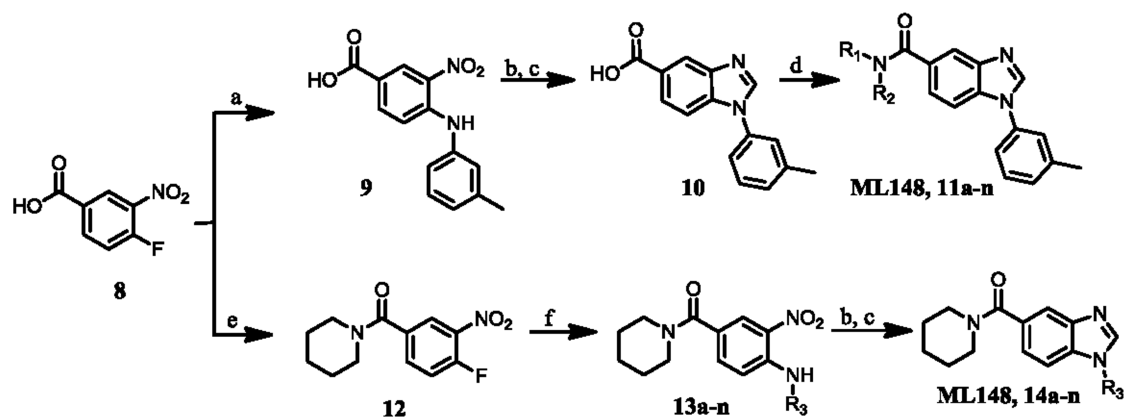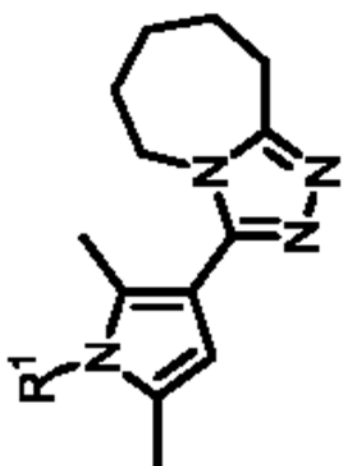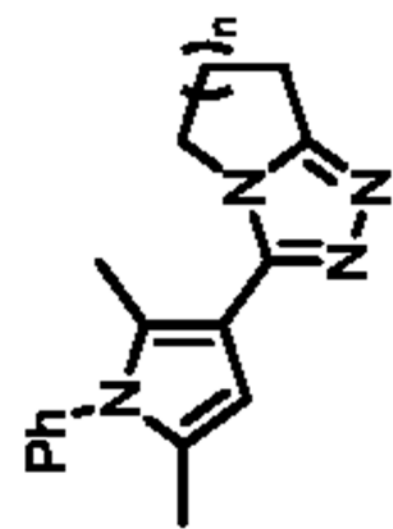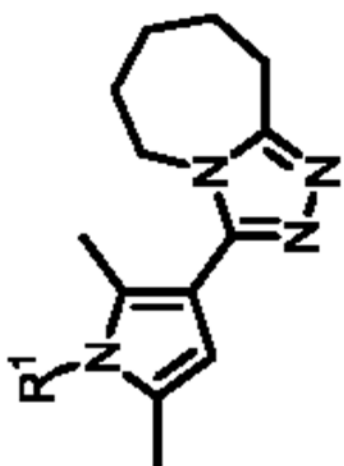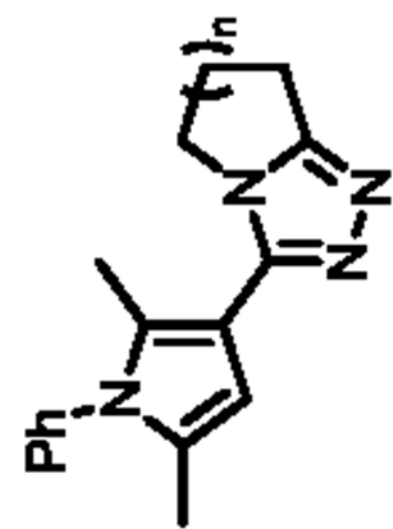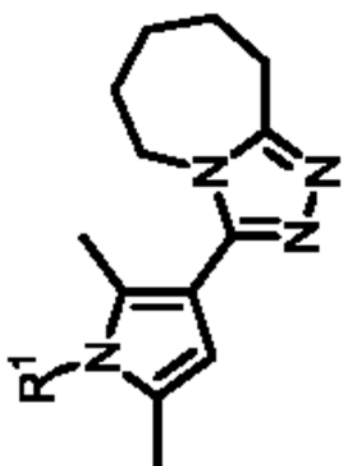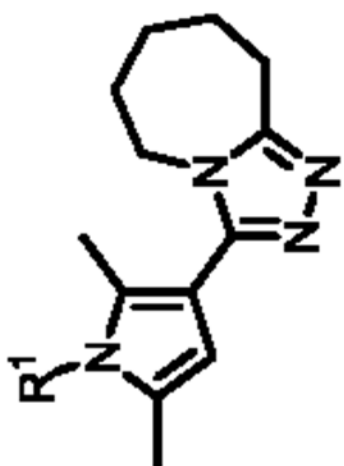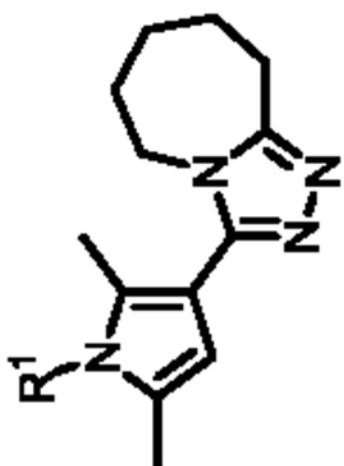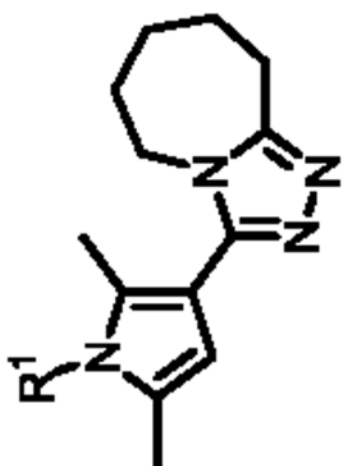
Scheme 4.
Reagents and conditions: (a) *o*-toluidine, NMP, 60 °C; (b) hydrazine, Ra-Ni, MeOH, 23 °C; (EtO)₃CH, TsOH, THF, MW, 120 °C; (d) R₁R₂NH or R₃NH₂, HATU, DIPEA, DMF, 23 °C; (e) (COCl)₂, DMF, DCM, 23 °C, then piperidine-HCl, DCM, 23 °C; (f) R₃NH₂, DIPEA, NMP, 120 °C.

Table 1

SAR of **ML149** and related analogues.
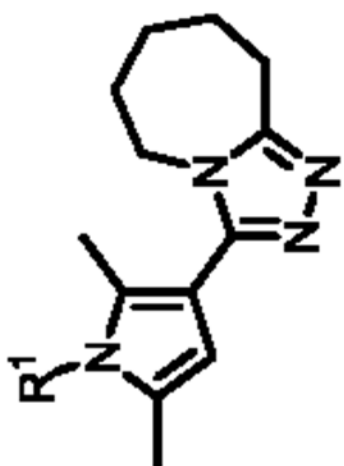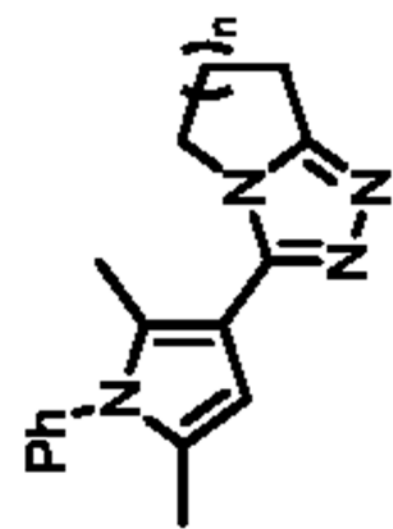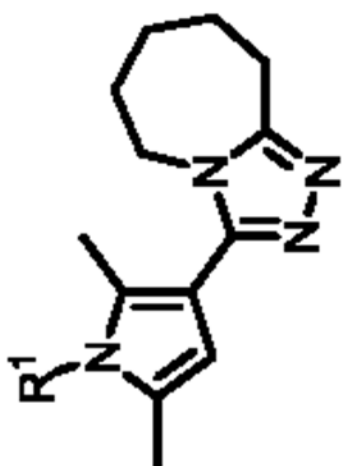

Compound	R¹	IC$_{50}$ (nM)[a]
ML149	phenyl	54
4a	3,4-Cl-phenyl	22
4b	3-Cl-phenyl	34
4c	4-Cl-phenyl	38
4d	4-Br-phenyl	48
4e	4-F-phenyl	121
4f	3-CF$_3$-phenyl	48
4g	4-CF$_3$-phenyl	68
4h	4-Me-phenyl	34
4i	3-CN-phenyl	76
4j	4-CN-phenyl	96

Compound	n	IC$_{50}$ (nM)[a]
6a	1	3040
6b	2	192
6c	4	242
6d	5	383

Compound	R²	IC$_{50}$ (nM)[a]

Compound	R^1	IC$_{50}$ (nM)^a
4k	4-OMe-phenyl	86
4l	4-NO$_2$-phenyl	108
4m	4-tBu-phenyl	136
4n	4-CO$_2$Et-phenyl	38
4o	2-pyridine	1078
4p	3-pyridine	271
4q	4-pyridine	383
4r	1-naphthalene	108

Compound	n	IC$_{50}$ (nM)^a
7a		607
7b		3827
7c		681

a determined using the HTS enzymatic assay and tested in triplicate.

Table 2

SAR of **ML148** and related analogues.
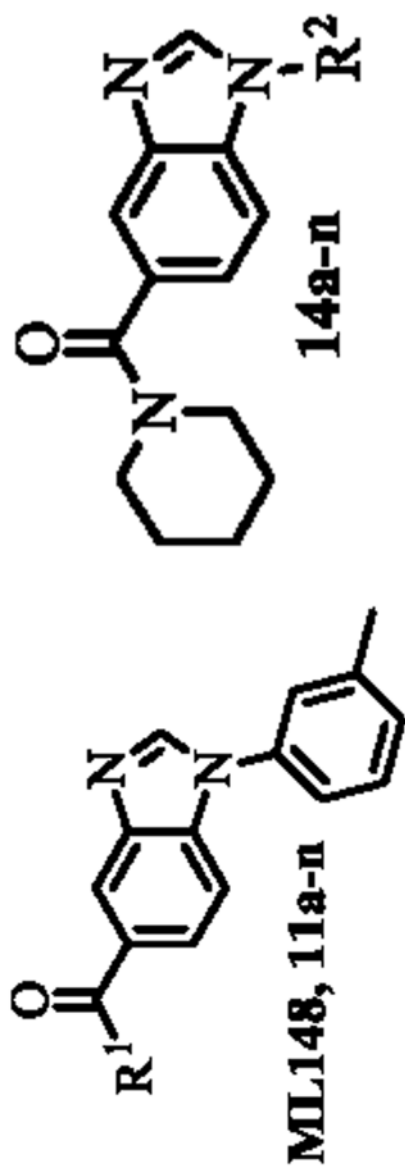
Compound	R[1]	IC$_{50}$ (nM)[a]	Compound	R[2]	IC$_{50}$ (nM)[a]
ML148		19	**14a**	phenyl	22
11a		22	**14b**	2-OMe-phenyl	27
11b		271	**14c**	3-Cl-phenyl	12

ML148, 11a–n / 14a–n
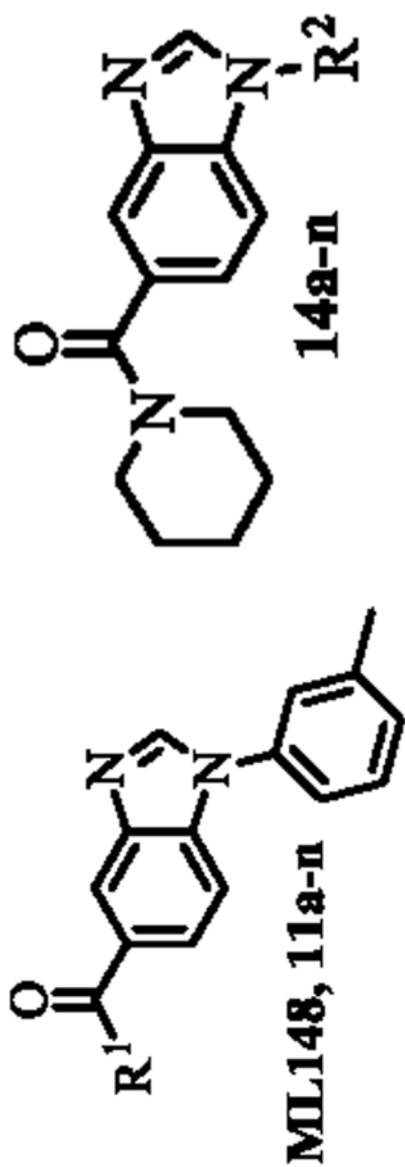
Compound	R^1	IC$_{50}$ (nM)[a]	Compound	R^2	IC$_{50}$ (nM)[a]
11c	(3-isopropylpiperidine)	48	14d	3-OMe-phenyl	19
11d	(3,3-dimethylpiperidine)	68	14e	3-CF$_3$-phenyl	48
11e	(3-CF$_3$-piperidine)	68	14f	3-iPr-phenyl	68
11f	(4-Br-piperidine)	76	14g	3-tBu-phenyl	171

ML148, 11a–n

14a–n
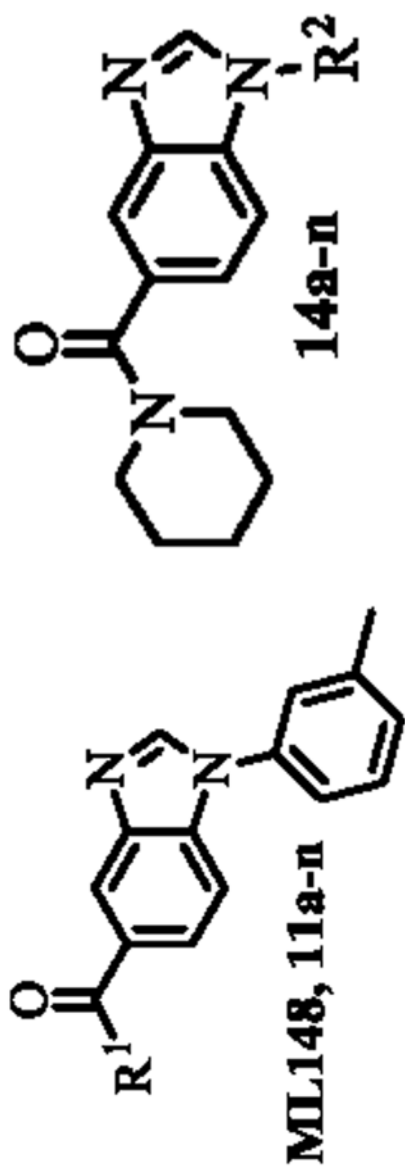
Compound	R¹	IC_{50} (nM)[a]	Compound	R²	IC_{50} (nM)[a]
11g	(F₃C-piperidine)	1524	14h	4-Me-phenyl	19
11h	(diethylamino)	383	14i	4-Cl-phenyl	22
11i	(pyrrolidine)	383	14j	4-OMe-phenyl	19
11j	(Ph-piperidine)	429	14k	4-CF₃-phenyl	86
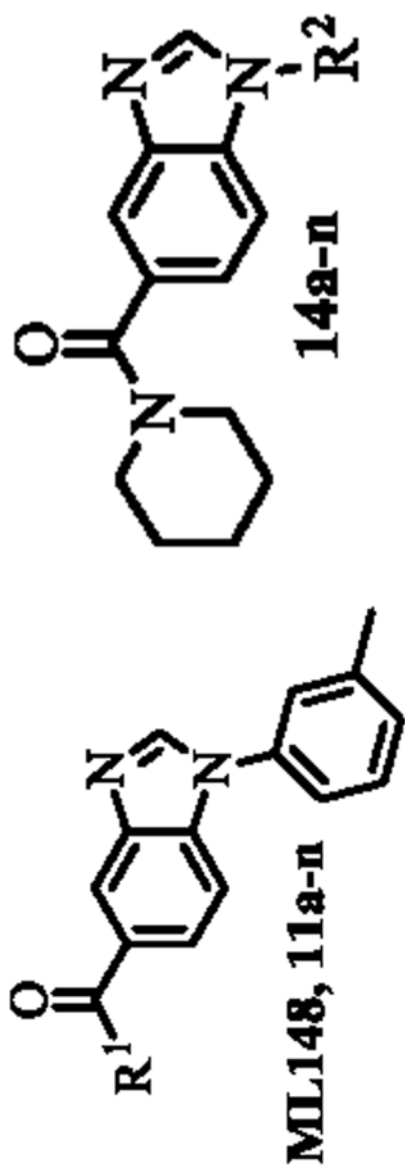
Compound	R^1	IC_{50} (nM)[a]	Compound	R^2	IC_{50} (nM)[a]
11k		961	14l	4-tBu-phenyl	54
11l		1358	14m	tBu	34
11m		2710	14n	nBu	68
11n		3040			

[a] determined using the HTS enzymatic assay and tested in triplicate.

Table 3

In vitro ADME properties of selected analogues of **ML149** and **ML148**.

Compound	IC$_{50}$ (nM)^a	Permeability (10^{-6} cm/s)^b	Kinetic solubility (μM)^c	RLM T$_{1/2}$ (min)^d
ML149	112	599	>45	n.d.
4a	22	1646	32	1.9
4b	34	1100	37	2.0
4f	48	1512	33	1.9
4h	34	1330	28	1.8
4i	76	229	>49	8.1
ML148	19	1196	>47	7.3
11d	68	2265	5.6	1.8
14c	12	895	>50	6.4
14e	48	1346	>55	4.4
14j	19	624	>50	23

^{a}represents the IC$_{50}$ against HPGD in the HTS enzymatic assay.

^{b}represents the PAMPA permeability at pH 7.4.

^{c}represents the kinetic aqueous solubility in PBS buffer (pH 7.4) as measured by UV quantification.

^{d}represents the T$_{1/2}$ in rat liver microsomes (RLM) in the presence of NADPH.

Table 4

PGE$_2$ produced in A549 and LNCaP cells.

Compound	IC$_{50}$ (nM)[a]	A549 cells AC$_{50}$ (μM)[b]	A549 cells % Induction[c]	LNCaP cells AC$_{50}$ (μM)[b]	LNCaP cells % Induction[c]
ML149	54	0.743	106	2.80	73
4a	22	0.296	110	0.352	105
4b	34	0.590	114	0.558	68
4f	48	2.09	145	2.22	44
4h	34	0.166	107	0.703	71
4i	76	2.64	350*	1.77	63
ML148	19	0.469	129	0.884	62
11d	68	0.743	127	4.43	53
14c	12	0.372	170	0.222	85
14e	48	2.64	173	2.80	70
14j	19	0.662	174	0.884	69

[a] represents the IC50 against HPGD in the HTS enzymatic assay;

[b] represents the half-maximal concentration in the PGE2 production assay;

[c] represents the percentage induction of PGE2 production;

* the titration curve was incomplete.